The 2009 IEEE/RSJ International Conference on
Intelligent Robots and Systems
October 11-15, 2009 St. Louis, USA

Pick-and-Place Nanomanipulation with Three-Dimensional Manipulation Force Microscopy

Hui Xie, *Member, IEEE,* Juan Camilo Acosta, *Student Member, IEEE,* Dogan Sinan Haliyo, and Stéphane Régnier

Abstract— **Applications of the conventional atomic force microscope (AFM) succeeded in manipulating nanoparticles, nanowires or nanotubes by widely used pushing or pulling operations on a single plane. However, pick-and-place nanomanipulation is still a challenge in the air. In this paper, a modified AFM, called three-dimensional (3D) manipulation force microscope (3DMFM) was developed, aiming to achieve the pick-and-place in the air. This system mainly consists of two microcantilevers and each is quipped with a nanopositioning device and an optical lever, constructing a nanotweezer with capabilities of picking and releasing nanoobjects with force sensing. Before the 3D manipulation, one of the cantilevers is employed to position nanoobjects and locate the tip of another cantilever by image scanning, then these two cantilevers fit together as a nanotweezer to grasp, transport and place the nanoobjects with real-time force sensing. In pick-and-place experiments, silicon nanowires (SiNMs) with different diameters were manipulated and 3D nanowire crosses were achieved. 3D nanomanipulation and nanoassembly in the air could become feasible through the newly developed 3DMFM.**

I. Introduction

Pick-and-place nanomanipulation is a significant technique on 3D nanostructure fabrication since it is an indispensable step in the "bottom-up" building process. It is also a promising nanofabrication technique to combine advantages of the "bottom-up" and the "top-down" methods for complex 3D nanostructures building. Nanostructures have been manipulated, assembled and characterized by integrating nanomanipulators or nanogrippers into scanning electron microscopes (SEM) and transmission electron microscopes (TEM) [1–4]. Both the SEM and the TEM provide a vacuum environment where the van der Waals force is the main force to be overcome during the manipulation. 3D manipulation could also be achieved with optical tweezers, because in this case the emergence of the liquid greatly reduces the often strong adhesion forces [5, 6]. However, pick-and-place manipulation is still a great challenge in air due to the presence of strong adhesion forces [7]. In this case, the main difficulties in completing a sufficient 3D manipulation in air are fabricating such sharp end-effectors with enough grasping forces as well as capabilities of sensing and control of strong interactions between the object and the tool or the substrate.

Manuscript received March 1, 2009; This work has been supported by the French National Agency of Research, through the PACMAN and NANOROL projects.

Authors are with the Institut des Systèmes Intelligents et Robotique (ISIR), Université Pierre et Marie Curie-Paris VI/CNRS, 4 Place Jussieu, 75005 Paris, France. (e-mail: xie@robot.jussieu.fr).

Compared with the SEMs and the TEMs, the AFM based nanomanipulation in the actual use has much more flexibility in applications to various nanoobjects in different environments-air, liquid and vacuum. However, conventional AFM based nanomanipulation strategies are restricted to push and pull nanoobjects on a single surface [8–12]. The pick-and-place manipulation of nanoobjects in air is still unresolved, although vertical pickup of atoms have be fulfilled by a electric field trapping [13], van der Waals forces [14, 15], tunneling current induced heating and inelastic tunneling vibration [15]. Grasping nanoobjects using two-tip carbon nanotube (CNT) tweezers has been demonstrated [16], but the alignment of the CNTs remains a challenge and capabilities of the CNT tweezer in overcoming great adhesion forces in air need to be validated. Therefore, a 3D nanomanipulation system is crucial in achieving the pick-and-place operation in the 3D nanostructures building.

In this paper, we have developed a two-tip AFM based manipulation system, called 3D manipulation force microscope (3DMFM). This system can be used as a conventional AFM to image, push and pull nanoobjects, and, more importantly, to achieve the pick-and-place operation with sufficient interaction force sensing and control during the manipulation. The 3DMFM mainly consists of two collaborative cantilevers with protrudent tips and correspondingly two sets of nanopositioning devices and optical levers. In order to locate tips and the nanoobjects, one of these two tips is employed to fulfill a topography scan on another tip and the nanoobjects, obtaining position information of nanoobjects and the tips before manipulation. Once the image scanning is ready, a nanotweezer is constructed by these two tips to achieve a procedure of 3D nanomanipulation with steps of contact detecting, grasping, picking up, transporting and releasing.

We have used the developed 3DMFM to build nanowire crosses by manipulating two types of cone-shaped silicon nanowires (SiNWs) with diameters of 15 nm (top) $\sim$ 70 nm (root) and 25 nm (top) $\sim$ 200 nm (root). Compared with other means of pick-and-place nanomanipulation achieved in the SEM and the TEM, 3D manipulation process using the developed 3DMFM is more controllable due to the real time interactive force sensing and with much more flexibility in different manipulation environment for various nanoobjects.

II. System Configuration of the 3DMFM

The 3DMFM is equipped with an optical microscope (Olympus BX50WI) and two sets of devices commonly used

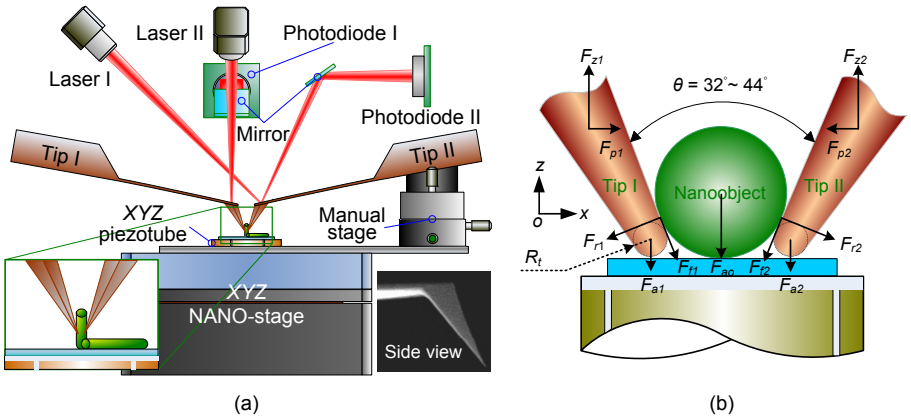

Fig. 1. (a) System configuration of the 3DMFM. (b) pick-and-place manipulation scheme with a "nanotweezer" constructed from two nanotips.

in a conventional AFM, mainly including two cantilevers with two sets of nanopositioning devices and optical levers. As shown in Fig. 1 (a), one *XYZ* piezoelectric actuated nanostage (MCL Nano–Bio2M) with a maximum scan range of 50 μm $\times$ 50 μm $\times$ 50 μm and a *XYZ* piezotube (PI P–153.10H) with a scan range of 10 μm $\times$ 10 μm $\times$ 10 μm are used. Note that hysteresis of the piezotube are well compensated by PI operator [17, 18]. The AFM cantilevers with protrudent tips (ATEC–FM), as shown in right inset of Fig. 1 (a), are employed as end-effectors for image scanning and manipulation. Two sets of optical levers, typically composed of a laser and a quadrant photodiode that is believed to be more sensitive and reliable detection device than other means [19], are arranged on two vertical planes and used to detect actions of cantilevers during the manipulation, as shown in Fig. 1 (a). The configuration could be described in detail as follows:

1) Cantilever I, employed as an imaging tip before manipulation and then a manipulating end-effector, is fixed on an *XYZ* micropositioning stage (not shown in Fig. 1). On the other hand, Cantilever II, as a manipulating end-effector supported by an *XYZ* manual microstage for coarse positioning, is mounted on the *XYZ* nanostage.
2) The *XYZ* piezotube, fixed on the *XYZ* nanostage, is used to support and transport samples.
3) A typical pick-and-place nanomanipulation scheme is depicted in Fig. 1 (b), in which a "nanotweezer" with a clamping angle of $32^{\circ} - 44^{\circ}$, constructed from the cantilever I and the cantilever II and each with mounting angle of $6^{\circ} - 12^{\circ}$, is utilized to pick up and place the nanoobject to its target position.

III. Pick-and-Place Schemes

A. Manipulation Protocol of the 3DMFM

Nanowires and nanotubes are being intensively investigated as the promising nanomaterials for applications in nanooptics, nanoelectronics and nanostructures in NEMS. Thus, a manipulation protocol of the 3DMFM is made for a specific application of the nanowires or the nanotubes deposited on the substrate. However, applications of the protocol also can be extended to the pick-and-place operations on, for example nanoparticles dispersed on the substrate. As seen in Fig. 2 (a), a pick-and-place procedure mainly involves:

1) System Initialization: Set each axis of the nanostage and the piezotube on a proper position. This setting will provide enough displacement for the nanoobjects manipulation within an image scanning area. Then locate Tip II (on the right) by local scanning using Tip I after a coarse positioning under the optical microscope .

2) Image Scanning Using Tip I: Once the locating on Tip II is ready, Tip I (on the left) is employed to fully scan the area of interest, obtaining a topographic image which contains nanoobjects to be manipulated and Tip II. The scanning area on Tip II is determined by the height of the nanoobjects, which should has a comparative maximum image height with the nanoobjects. This step is depicted in Fig. 2 (a)-I, in which the nanostage is used track the topography during the image scanning. The scanning image contains two nanowires and the end of Tip II, as shown in Fig. 2 (b).

3) Relocate Tip II: If the nanomanipulation is performed in an uncontrolled environment, the thermal drift is a noticeable cause of the positioning errors. Therefore, after a long-playing image scanning, relocating Tip II is quite necessary to succeed in constructing of the "nanotweezer".

4) Approach Tip II to One Nanowire: Keep a tiny gap (typically 5 nm $\sim$ 20 nm) between Tip II and the substrate, then approach Tip II to one nanowire by moving the piezotube on the *X* axis. An actual contact with the nanoobject can be predicted by a tiny force load on Tip II. This step is depicted in Fig. 2 (a)-II.

5) Approach Tip I to Tip II: Similarly, approach Tip I to Tip II to form a "nanotweezer" by moving the nanostage on the *X* axis until an actual contact with the nanoobject estimated by a tiny force load on Tip I. This step is depicted in Fig. 2 (a)-III.

6) Pick up, Transport and Place: Once the "nanotweezer" is constructed on the step 5), the nanowire is picked up, transported and placed by moving piezotube on the *X*, *Y* or

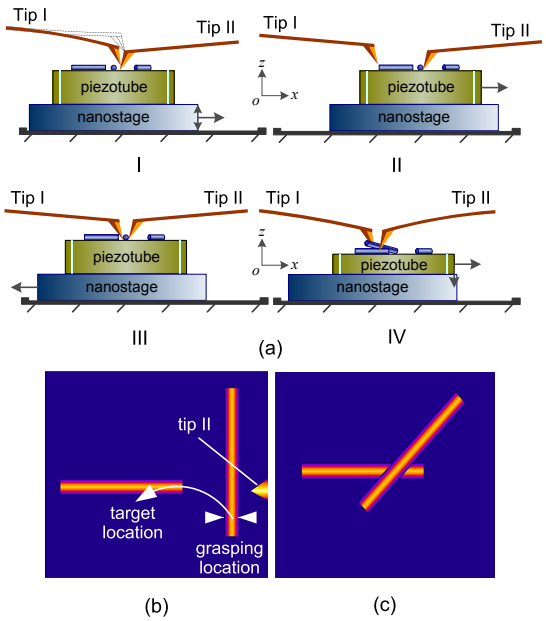

Fig. 2. Protocol of pick-and-place of nanowires. (a) Four steps from step I to IV are involved. (b) Locations of nanowires and Tip II are recorded by a simulated pre-image scan. (c) A nanowire nanocross is built.

Z axes with proper distances depending on dimensions of the nanowire and the location of the destination.

B. Force Sensing During Manipulation

In order to measure the interactive forces between the tips and the nanoobjects, as shown in Fig. 1 (b), the 3D interactive forces on Tip I in the defined frame can be determined by normal signals from the photodiode by:

$$F_{z1} = F_{f1}\cos\frac{\theta}{2} + F_{r1}\sin\frac{\theta}{2} + F_{a1} \tag{1}$$

$$F_{p1} = F_{r1}\cos\frac{\theta}{2} - F_{f1}\sin\frac{\theta}{2} \tag{2}$$

where F_{z1} and F_{p1} are the bending forces applied respectively on the Z axis and the X axis, F_{a1} is the adhesive force between Tip I and the substrate, F_{r1} is a repulsive force and F_{f1} is a friction force between Tip I and the nanoobjects. The F_{f1} includes friction μF_{r1} contributed from the repulsive force and the shear force F_s. These two parts can be simplified as $\mu^{'}F_{r1}$, here $\mu^{'}$ is a friction coefficient. In the actual use, a clamping angle $40°$ and a normal $\mu^{'} = 0.3$ are used [20]. Thus, from (1) and (2), F_{z1} and F_{p1} can be solved as:

$$F_{z1} = 0.623F_{r1} + F_{a1} \tag{3}$$

$$F_{p1} = 0.837F_{r1} \tag{4}$$

The bending angular deformation ϕ associated with a torque M applied on the end of the cantilever can be calculated as:

$$\phi = \frac{ML}{2EI} \tag{5}$$

where L is the beam length of the AFM cantilever, E is Young's modulus of the cantilever, I is moment of inertia on the cantilever's cross-section area. A torque M_1 is generated from the F_{z1} with a long turning lever $L = 225$ μm. In contrast, the torque M_2 generated from the F_{p1} is just with a turning lever of the tip length $l = 10$ μm. From (3) and (4), the cantilever moments associated with the normal signal output of the photodiode can be estimated as:

$$M_2 \leq 0.06M_1 \tag{6}$$

Finally, from (6), it can be found that the contribution of the normal force signal from the F_{p1} is less than 6% of that of the F_{z1}. Therefore, the F_{z1} can be simplified as:

$$F_{z1} = \beta_1\Delta V_1 - F_{a1} \tag{7}$$

where β_1 ΔV_1 are the normal force sensitivity and the voltage response of the photodiode on Tip I, A similar result can be deduced on Tip II. Once the F_{z1} and F_{z2} are known, the adhesion force on the nanoobject F_{ao} can be estimated as:

$$F_{ao} = F_{z1} + F_{z2} = (\beta_1\Delta V_1 + \beta_2\Delta V_2) - (F_{a1} + F_{a2}) \tag{8}$$

where β_2 and ΔV_2 are respectively the normal force sensitivity and the voltage response of the photodiode on Tip II, F_{a1} and F_{a2} are typically the pull-off forces on each tip.

C. Manipulation Limits of 3DMFM

In the proposed 3DMFM, the minimum size of nanoobjects can be manipulated is determined by the tip size of the cantilever. As shown in Fig. 3, in order to complete the grasping, the angle α and the dig-in distance ξ should be positive, which can be calculated via:

$$\alpha = \arcsin\left(\frac{R_o - R_t}{R_o + R_t}\right) \tag{9}$$

$$\xi = R_o(1 - \cos\alpha) \tag{10}$$

where R_o and R_t are the radius of the nanoobject and the tips, respectively. In the actual use, the effective dig-in distance ξ will be reduced by the cantilever's normal deflection due to F_{z1}. The lateral tip stiffness is typically two to three orders of the magnitude larger than the normal stiffness of the cantilever [21]. Therefore, the deformation on the tip can be neglected and Tip I deflection $\xi^{'}$ on the X axis can be calculated as:

$$\xi^{'} = -\frac{F_{z1}}{k_1}\left(\frac{3l}{2L}\cos\gamma + \tan\gamma\right) \tag{11}$$

where δ_{n1} is the normal deflection on Tip I due to the force F_{z1}, L and l are lengths of cantilever's beam and tip, respectively. Here, deflection caused by the force F_{p1} is neglected as mentioned above. Therefore from (9)–(11), to achieve grasping operation by the nanotweezer, the effective dig-in distance could satisfy $\xi + \xi^{'} > 0$. Thus, the minimum radius of the nanoobject R_{min} can be calculated via:

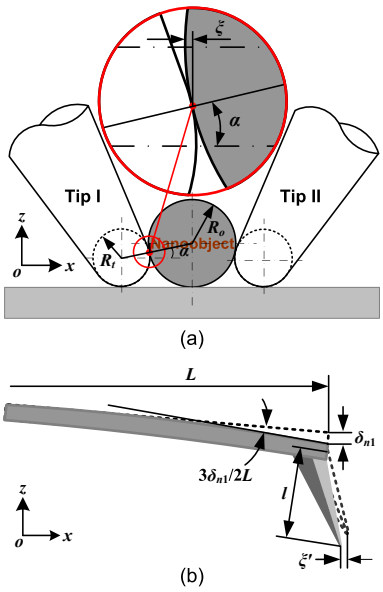

Fig. 3. Schematic diagram for manipulation limits calculation.

$$R_{\min}\left(1-\sqrt{1-\frac{(R_{\min}-R_t)^2}{(R_{\min}+R_t)^2}}\right)=\frac{F_{z1}}{k_1}\left(\frac{3l}{2L}\cos\gamma+\tan\gamma\right) \tag{12}$$

For example, during the pickup, if the maximum $F_{z1} = 50$ nN, $R_t = 8$ nm, $k_1 = 4$ N/m, $\gamma = 5°$, $L = 250$ μm and $l = 10$ μm, the minimum diameter of the nanoobjects that can be picked up is $D_{min} = 2R_{min} = 39.4$ nm. If a worn tip with $R_t = 15$ nm is used, the minimum diameter of the nanoobjects will increase to $D_{min} = 61.1$ nm. Actually, it is hard to achieve this limit due to chemical dirt always attaching on the nanoobject's root, which is on the way of grasping operation leading to a decrease on the effective dig-in distance. However, a sharper AFM tip extended with single-walled carbon nanotubes or larger structures called multi-walled carbon nanotubes may be a promising breakthrough in the grasping limits described above [22]. Another possibility on the limit extension is to manipulate the suspended nanoobject, because in this case more space will be provided for achieving a closer grasping gap between the tips, bypassing the restriction on the dig-in distance ξ and thereby enabling pick up the nanoobject with a much smaller diameter than the tip diameter.

IV. 3D Nanomanipulation of Silicon Nanowires

A. Sample Preparation

In experiments, the silicon nanowires (SiNWs) were attached to a newly cleaned silicon wafer with a 300 nm dioxide coating. Two types of cone-shaped SiNWs with different diameters from 15 nm (top) $\sim$ 70 nm (root) and 25 nm (top) $\sim$ 200 nm (root) were manipulated.

B. Contact Detection

The contact detection is a significant step for a successful grasping of the nanoobject. In order to detect the nanoobject-tip interaction in the operation of grasping, a tiny gap between the tip and the substrate, for example, 5 nm $\sim$ 20 nm, should be kept when the tip approaches the nanoobject. As the tip approaches and further "digs into" the root of the nanoobject after contact, the gap enables cantilever's flexure deformation for a bending force sensing.

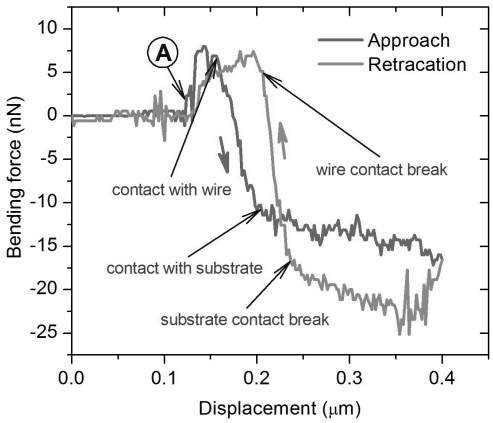

Fig. 4. Contact detection by bending force sensing applied on Tip II during the grasping operation.

Fig. 4 shows an example of the contact detection on Tip II by manipulating a silicon nanowire on the grasping point A–A as seen in Fig. 6 (a). The curve starts from non-contact state neither contact with substrate nor with the nanowire. As the Tip is moved toward the nanowire further, the cantilever is bent upward a little (about 3 nm) leading to positive force responses after "A" position. Two factors could contribute to this positive response: chemical dirt on the border of the nanowire and adhesion forces from the nanowire. The tip starts to dig into the root of the nanowire as its positive response reaches the first peak of 7.4 nN and contact with nanowire. In this part, the bending force decreases rapidly before the tip contacts with the substrate. The further push leads to a pushing operation on the nanowire and causes slow decreases of the bending force due to the tip deformation. During the retraction, after a contact break with the substrate, the bending force sharply reaches a positive peak with a slightly smaller value than the former peak. Eventually, the tip returns to the position "A" with the same force response. However, the regular snap-in and pull-off of the tip-substrate contact do not occur due to a delicate balance between the adhesion forces from the nanowire and the substrate.

The force response described in the Fig. 4 is sufficiently to detect not only the contact between the tip and the nanoobject, but the grasping state. As Tip II-nanowire contact is ready, Tip II retraces with a displacement of 5 nm $\sim$ 10 nm in order to keep a tiny gap between Tip II and the substrate, enabling the detection of grasping state as Tip I contact the nanowire with a slightly further pushing.

C. Force Sensing in pick-and-place

Fig. 5 shows a peeling force spectroscopy curve on Tip II for the pick-up and releasing operation of the same nanowire with the same grasping point A–A (shown in Fig. 6 (a)). The

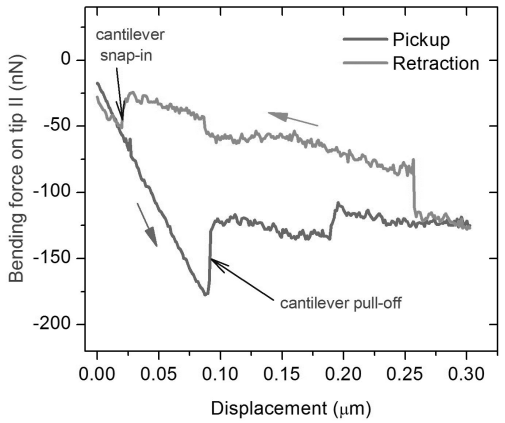

Fig. 5. Force detection on Tip II during the pick-up operation.

curve starts from contact state among the tips, the substrate and the nanowire. During the pickup, when the position reaches 88 nm, the cantilever pulls off the substrate with an adhesion force of 52 nN, a typical pull-off force of the common cantilever, and the force curve returns to -125 nN. As the tips move up further, the force magnitude keeps slightly decreasing to a value of -136 nN at 188 nm. After this point, the magnitude of the force suddenly reduces to -110 nN, forming a tiny force peak of 5 nN. Further pickup leads to another slow decrease of the peeling force to -125 nN at 302 nm. The retraction starts from this point and at the first part of the retraction, as the tips approach the substrate, the force slightly increase form -126 nN to -118 nN at 258 nm. A sudden increase of 43 nN occurs at this point with the further retraction. Further retraction leads to a continue increase except for a weak fluctuation between 135 nm $\sim$ 81 nm. Snap-in occurs at 21 nm after a mild decrease of the force. The snap-in force reaches -21 nN. Upon still further retraction, the magnitude of the normal force of Tip II approaches the previous grasping state. The force responses on Tip I are similar in the curve shape except for differences on the signal magnitude due to different force sensitivities on each tip and an uneven grasping due to asymmetric alignment of the nanowire related to the grasping direction.

Once such a force spectroscopy curve occurs during the picking up operation, a stable grasping can be validated for further transportation and releasing operations. Details of the force responses during the transportation and the releasing operations of the nanowire are shown in Fig. 6 (d).

D. Manipulation Results

Fig. 6 exhibits the 3D manipulation of the SiNWs with a diameter of 25 nm (top) $\sim$ 200 nm (root). A scanned image 9 μm $\times$ 9 μm is shown in Fig. 6 (a), which includes the topographic image of several nanowires, and of course also involves the local image of Tip II (see the insert). A Grasping location of the nanowire are marked with a short green line A–A, where the nanowire has a height of 166 nm, as seen in the top insert. Fig. 6(c) shows the re-scanning image after pick-and-place manipulation. It can be found that the nanowire has been successfully transported and placed onto another nanowire to build a nanocross. A full force curve was recorded from the force response on Tip II, as shown in Fig. 6 (b). The force curve exhibits four steps, including grasping, picking up, transporting and placing. Once the silicon nanowire was reliably grasped, piezotube moved down 650 nm with a velocity of 65 nm/s and the photodiode voltage output decreased to 0.24 V before the third step. In this step, the silicon nanowire was transported a distance of 4.6 μm on the X axis with a velocity of 120 nm/s and 0.18 μm on the Y axis with a much smaller velocity of 4.8 nm/s. During the transport, a disorder (within a red circle) occurred due to its contact with the supporting nanowire before releasing. This is a explanation to the force response on the last step, which has no distinct change until the cantilever snap-in on the substrate because the manipulated nanowire had been staked. piezotube moved up with a velocity of 100 nm/s until Tip II was slightly bent upward leading a positive response of 0.015 V. Lastly, Tip I and Tip II separated by moving the nanostage on the X axis to release the nanotweezer.

Another type of cone-shaped SiNWs with diameters of 15 nm (top)$\sim$ 70 nm (root) were manipulated as seen in Fig. 7. After image scan shown in Fig. 7 (a), three silicon nanowires were selected and the manipulation locations were placed near the top, the root and on the middle part of the SiNWs, marked by short green lines B–B, C–C and D–D, respectively. The SiNWs heights on these locations are 46 nm, 66nm and 58 nm, respectively. In the first grasping on the location B–B, after successful contact detection on Tip II, as Tip I approach the nanowire to form a nanotweezer, the "dig into" response as shown in Fig. 5 did not occur, that meant the first silicon nanowire could not be picked up but be pushed by Tip I, which is verified on the Fig. 7 (b). Two factors could contribute the failure of the grasping: some chemical dirt on the way of "dig into" and another significant factor associated with the manipulation limits as described in section C of part III was that the worn Tip I after image scanning reached its limit for pickup manipulation. On the second manipulation location C–C, the 3DMFM succeeded in pick-and-place manipulation and building a nanocross, as shown in the zoom image Fig. 7 (c). A similar force response during the manipulation could be obtain as Fig. 6 (b) shows, just the magnitude of the force was in the order of several to tens nN. Another failure happened in the manipulation of the third nanowire on its middle part on location D–D. Force detection indicated the 3DMFM succeeded the grasping, but during the pick-up or transportation process, the nanowire stuck to Tip II. This failure was confirmed by abnormal behavior on local scan with Tip II on tapping mode.

V. Conclusion

It is well known that the pick-and-place operation is still a challenge in nanomanipulation in air . Fortunately, the newly developed 3D manipulation force microscope (3DMFM) has achieved this type of pick-and-place nanomanipulation using a nanotweezer constructed by two AFM cantilevers. In order

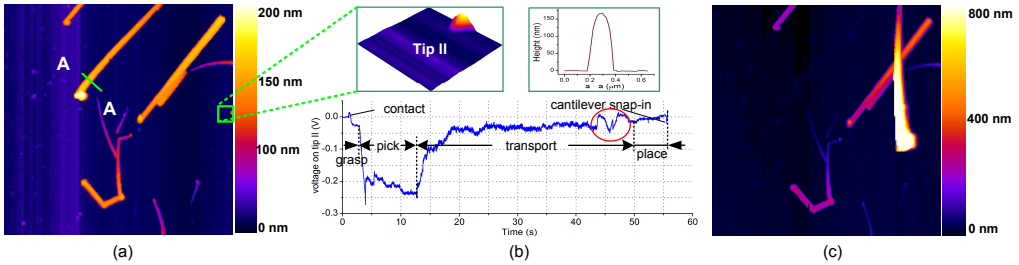

Fig. 6. Building a nanocross using SiNWs with diameters of 25 nm (top) $\sim$ 200nm (root). (a) A pre-scanned image. (b) A full force curve on Tip II. Inserts show the zoom topography of Tip II and height information at A–A. (c) A post-manipulation image shows that a nanocross has been built.

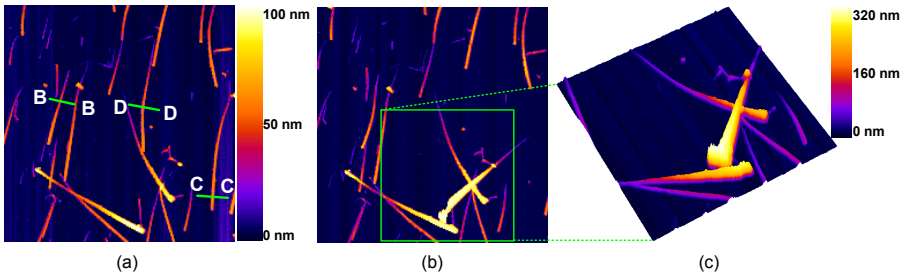

Fig. 7. Building a nanocross using SiNWs with diameters of 15 nm (top) $\sim$ 70nm (root). (a)A pre-scanned image. (b)A post-manipulation image shows manipulation results. (c) A zoom topography of the nanocross.

to validate the manipulation ability of the 3DMFM, two types of cone-shaped SiNWs were manipulated and two nanowire crosses were achieved. Moreover, force recording during the pick-and-place manipulation provides valuable data in the understanding of the nanomechanics and nanophysics. As a result, the 3DMFM has made the 3D nanomanipulation and nanoassembly, such as constructing 3D nanostructures, building 3D nanodevices, and revealing nanomechanics phenomena feasible.

REFERENCES

[1] T. Fukuda, F. Arai, and L. X. Dong, "Assembly of nanodevices with carbon nanotubes through nanorobotic manipulations," *Proc. IEEE*, vol. 91, no. 11, pp. 1803–1818, 2003.

[2] L. X. Dong, F. Arai, and T. Fukuda, "Electron-beam-induced deposition with carbon nanotube emitters," *Appl. Phys. Lett.*, vol. 81, no. 10, pp. 1919–1921, 2002.

[3] L. X. Dong, F. Arai, and T. Fukuda, "Destructive constructions of nanostructures with carbon nanotubes through nanorobotic manipulation," *IEEE/ASME Trans. Mechatron.*, vol. 9, no. 2, pp. 350–357, 2004.

[4] K. Molhave, T. Wich, A. Kortschack, and P. Boggild, "pick-and-place nanomanipulation using microfabricated grippers," *Nanotechnology*, vol. 17, no. 10, pp. 2434–2441, 2006.

[5] T. Yu, F. C. Cheong, and C. H. Sow, "The manipulation and assembly of CuO nanorods with line optical tweezers" *Nanotechnology* vol. 15, no. 12, pp. 1732–1736, 2004.

[6] L. Bosanac, T. Aabo, P. M. Bendix, and L. B. Oddershede, "Efficient optical trapping and visualization of silver nanoparticles," *Nano lett.*, vol. 8, no. 5, 1486–1491, 2008.

[7] Y. Rollot, S. Régnier, J. C. Guinot, "Simulation of micromanipulations: Adhesion forces and specific dynamic models," *Inte. J. Adhes. Adhes.*, vol. 19, no. 1, pp. 35–48, 1999.

[8] M. R. Falvo, R.M.I. Taylor, A. Helser, V. Chi, F.P.J. Brooks, S. Washburn, and R. Superfine, "Nanometre-scale rolling and sliding of carbon nanotubes," *Nature*, vol. 397, no. 6716, pp. 236–238, 1999.

[9] C. Baur, A. Bugacov, B. E. Koel, A. Madhukar, N. Montoya, T. R Ramachandran, A. A. G .Requicha, R. Resch and P. Will, "Nanoparticle manipulation by mechanical pushing: underlying phenomena and real-time monitoring," *Nanotechnology*, vol. 9, no. 4, pp. 360–364. 1998.

[10] R. Resch, D. Lewis, S. Meltzer, N. Montoya, B.E. Koel, A. Madhukar, A.A.G. Requicha, P. Will, "Manipulation of gold nanoparticles in liquid environments using scanning force microscopy," *Ultramicroscopy*, vol. 82, no. 1–4, pp. 135-139, 2000.

[11] M. Sitti, S. Horiguchi, and H. Hashimoto, "Controlled pushing of nanoparticles: modeling and experiments," *IEEE/ASME Trans. Mechatron.*, vol. 5, no. 2, pp. 199–211, 2000.

[12] Y. J. Yun, C. S. Ah, S. Kim, W. S. Yun, B. C. Park, and D. H. Ha, "Manipulation of freestanding Au nanogears using an atomic force microscope," *Nanotechnology*, vol. 18, no. 50, pp. 505304, 2007.

[13] L. J. Whitman, J. A. Stroscio, R. A. Dragoset, and R. J. Cellota, "Manipulation of adsorbed atoms and creation of new structures on room-temperature surfaces with a scanning tunneling microscope," *Science*, vol. 251, no. 4998, pp. 1206–1210, 1991.

[14] D. M. Eigler and E. K. Schweizer, "Positioning single atoms with a scanning tunneling microscope," *Nature*, vol. 344, no. 6266, pp. 524–526, 1990.

[15] P. Avouris, "Manipulation of matter at the atomic and molecular levels," *Accounts Chem. Res.*, vol. 28, no. 3, pp. 95–102, 1995.

[16] P. Kim and C. M. Lieber, "Nanotube nanotweezers," *Science*, vol. 286, no. 5447, pp. 2148–2150, 1999.

[17] P. Krejci and K. Kuhnen, "Inverse control of systems with hysteresis and creep," *IEE Proc.-Control Theory Appl.*, vol 148, no. 3, pp. 185–192, May 2001.

[18] B. Mokaberi, and A. A. G. Requicha, "Compensation of scanner creep and hysteresis for AFM nanomanipulation," *IEEE Trans. Autom. Sci. Eng.*, vol. 5, no. 2, pp.197–206, 2008.

[19] G. Meyer, and N. M. Amer, "Novel optical approach to atomic force microscopy," *Appl. Phys. Lett.*, vol. 53, no. 12, pp. 1045–1047, 1988.

[20] M. Varenberg, I. Etsion, and G. Halperin, "An improved wedge calibration method for lateral force in atomic force microscopy," *Rev. Sci. Instrum.*, vol. 74, no. 7, pp. 3362–3367, 2003.

[21] R. J. Cannara, M. Eglin, and R. W. Carpick, "Lateral force calibration in atomic force microscopy: A new lateral force calibration method and general guidelines for optimization," *Rev. Sci. Instrum.*, vol. 77, no. 5, pp. 053701, 2006.

[22] H. W. Lee, S. H. Kim, Y. K. Kwaka, and C. S. Han, "Nanoscale fabrication of a single multiwalled carbon nanotube attached atomic force microscope tip using an electric field," *Rev. Sci. Instrum.*, vol. 76, no. 4, pp. 046108, 2005.